Journal of Thermal Science Vol.31, No.5 (2022) 1773−1789

https://doi.org/10.1007/s11630-022-1683-4 **Article ID: 1003-2169(2022)05-1773-17**

Effect of Squealer Tip with Deep Scale Depth on the Aero-thermodynamic Characteristics of Tip Leakage Flow

BI Shuai, WANG Longfei*, WANG Feilong, WANG Lei, LI Ziqiang

Jiangsu Province Key Laboratory of Aerospace Power System, Nanjing University of Aeronautics and Astronautics, Nanjing 210016, China

Abstract: In this paper, the aero-thermal performance of squealer tips with deep-scale depth is numerically investigated in an axial flow turbine, which is compared with the squealer tip with traditional cavity depth. Numerical methods were validated with experimental data. The effect of cavity depth and tip clearance was considered. The numerical results show that for the squealer tip with conventional cavity depth, the size of the reflux vortex enlarges as the cavity depth increases. The velocity and uniformity of high entropy production rate (EPR) inside the cavity reduce obviously with the cavity developing into deep-scale. However, the increase of depth 10% of the blade span (*H*) leads to enlargement of cavity volume, which increases the total entropy production rate. And the overall dimensionless entropy production rate (DEPR) of gap and cavity obtains a maximum increase of 43.54% in contrast to the case with 1%*H* depth cavity. As a result, the relative leakage mass flow rate reduces by 20.6% as the cavity depth increases from 1% to 10%. Given the heat transfer, as the cavity significantly increases to 10%*H*, the enhanced cavity volume results in a more enormous cavity vortex with low velocity covering the floor, which weakens the convective heat transfer intensity and reduces the area of high heat transfer. The normalized average heat transfer coefficient at the cavity bottom reduces by 40.26% compared to the cavity depth of 1%*H*. In addition, the deep-scale cavity is more effective in inhibiting leakage flow at smaller tip clearance. The reduction amplitude of normalized average heat transfer coefficient at the squealer floor decreases as tip clearance increases, which reduces at most by about 72.6% for the tip clearance of 1%*H*.

Keywords: squealer tip, turbine aerothermodynamics, tip leakage flow, deep-scale depth, heat transfer, numerical methods

1. Introduction

There is relative movement between turbine rotor blades and casing in a gas turbine machine. The radial clearance could ensure the safe operation of the engine. So a part of high-temperature gas that does not participate in workflows through tip clearance, forming tip leakage flow (TLF).

The TLF forms leakage vortexes on the suction side of blade (SS), which leads to more significant flow loss. Among them, tip clearance leakage loss accounts for about 30% of the total loss [1]. Bunker [2] pointed out that the increase of clearance would result in turbine efficiency loss and outlet temperature increase. Due to the limitation of modern technology and fabrication, the absolute clearance of turbine tip could be controlled

Received: Jun 26, 2021 AE: AL-ABDELI Yasin Corresponding author: WANG Longfei E-mail: wlf@nuaa.edu.cn

Nomenclature

C_{ax}	axial chord of the blade
C_p	static pressure loss coefficient
d_i	depth of the squealer
H	span of the blade
h	heat transfer coefficient
h_{ave}	area-averaged heat transfer coefficient
Nu	Nusslet number
Q	Heat flux
$\overline{s}_{ij}$	strain rate tensor
W	width of squealer
ε	relative leakage mass flow rate
λ_T	turbulent heat transfer coefficient
μ_T	turbulent viscosity coefficient
τ	tip clearance height

Abbreviations

DEPR	dimensionless entropy production rate
EPR	entropy production rate
HPT	high-pressure turbine
LE	leading-edge of blade
PS	pressure side of blade
SS	suction side of blade
TE	trailing edge of blade
TKE	turbulent kinetic energy
TLF	tip leakage flow
TLV	tip leakage vortex
TPV	tip passage vortex

Subscripts

in/out	inlet/outlet of the computational domain
t	total

within a certain range. Therefore, the efficiency and temperature of small gas turbines were more sensitive to clearance.

The leakage flow formed by high-temperature gas in tip clearance not only causes leakage loss, but also makes the tip bear an extremely high thermal load. The oxidation and ablation of the tip directly affect the service life of the rotor blade. At present, the inlet working medium temperature of some gas turbines is close to 2000 K [3], which exceeds the material temperature limit of blade. Consequently, it is necessary to diminish the heat of tip. To cut down the flow loss and heat on the tip region, the tip structure design is vital.

Many scholars have conducted some research on the leakage flow of flat tip. Booth [4] pointed out that the gap leakage flow was similar to flowing through a long orifice plate. Yamamoto [5] experimentally further found that the interaction between secondary flows was enhanced with the flow deflection and clearance height increasing. In addition, Denton [6] proposed that the leakage flowed separated and attached to the tip surface, resulting in tip pressure-side separation bubbles. This complements the flow characteristics of tip leakage flow. While studying tip flow, heat transfer in the tip region has also attracted the extensive attention of scholars. Azad et al. [7] tested the temperature field of flat tip through experiments. The results showed that a high heat transfer area appeared on the tip toward the pressure side of blade (PS). Kwak [8] found that the leakage flow path through the gap affected the heat transfer distribution. The region of high heat transfer was near the PS, which was due to separation and reattachment of TLF. On the whole, inhibition of tip thermal load is still needed to change the distribution of leakage flow.

As a commonly used structure to restrain TLF, the squealer forms a “labyrinth like” seal at the blade’s tip. This reduces the pressure differential in the leakage flow, and effectively reduces the flow space between the rotor and the casing.

Bunker [2] found that a separation vortex appeared on the upper side of the squealer rim wall near PS; then it impinged to the cavity bottom near LE, forming a TLV in the cavity. This vortex developed towards TE and formed a blocking effect on clearance leakage. The leakage flow finally flowed out of the clearance near SS and formed a contraction flow on the squealer rim near SS, and then it mixed with the mainstream to create a leakage vortex.

Azad [9] found that when the leakage flow flowed through the TE of cavity with a relatively small width, the leakage flow may not reattach in the cavity. When the leakage flow flowed through LE of the cavity with a rather large width, the leakage flow may impinge on the rim surface near SS or the bottom surface of the cavity, and formed a backflow vortex on the rim wall near PS. Zeng et al. [10, 11] also confirmed that the TLF entered the cavity and created a reflux vortex through the PIV experiment and numerical simulation. Zhou and Hodson [12] showed that the squealer tip reduced heat compared to the flat tip as the gap was less than 2.5% chord.

After studying the characteristics of squealer tip clearance leakage flow, many scholars began to pay attentions to the cavity structure design. Given the influence of different placement positions of rims, Kavurmacioglu et al. [13] investigated the characteristics of partial (PSQ) and squealer tip (SQ), and found that SQ reduced leakage flow mass rate by 19.0%. Yang [14]

found that the sing suction-side squealer tip could effectively diminish Stanton numbers compared to the double squealer tip. In addition, Liu et al. [15] found SS squealer case performed best on reducing the heat transfer of tip among double squealer tip, PS squealer tip and SS squealer tip.

On that basis, there are some studies on different hybird tip structures, such as the squealer-winglet tip, squealer tip with inclined rim and squealer tip with ribs. Zhong et al. [16] discussed the control effect of tip winglet with squealer tip design on leakage for the compressor rotor. Cui et al. [17] investigated the effects of width of pressure-side winglet on tip flow in the compressor rotor. As the width of pressure-side winglet increases, the strength of leakage massflow was attenuated obviously. Similarly, hybird tip structures have been used in many turbine blade design studies. Zou et al. [18, 19] studied that the squealer tip with inclined pressure side squealer rim significantly reduced the TLF, which improved stage efficiency by 5%. Kim et al. [20] studied that the area-averaged heat transfer coefficient could be diminished by 13% for the inclined shelf squealer tip. Besides, some new hybrid structures could weaken the heat transfer distribution of tip. Yan et al. [21] found that squealer tip configured with pressure-side winglet diminished the heat transfer value by 10% compared to the conventional squealer tip.

In view of the research on squealer tip with rib layouts, Choi et al. [22] found that the vertical rib case performed best on reducing total pressure loss coefficients and local heat transfer. Du et al. [23] investigated aerothermal performance of the muti-cavity squealer tip. The results showed that the case of 5CST reduced the heat transfer coefficient the most by 17.5% compared to flat tip. Jiang et al. [24] investigated the aerothermal characteristics for different rib layouts. The results mentioned that the Case 5 (half rib structure in the actual squealer cavity) decreased the heat transfer by 11.3% in comparison to Case 1 (traditional squealer tip).

In addition to different blade tip structures, many scholars have focused on the influence of the cavity depth and rim width after the tip modification. Lee et al. [25] experimentally studied the effect of cavity depth on downstream losses. It is found that TLV decreases, and the interaction between TLV and TPV decreases with cavity depth increasing. Zhou [26] numerically studied that the size of the cavity vortex increases with cavity depth increasing. On this basis, some scholars studied the effect of cavity depth from another aspect. Shi et al. [27] investigated the aerothermal effect of cavity depth by using sensitivity analysis. The results confirmed that the cavity depth has a significant impact on leakage flow, which related to the scraping vortex was affected in the gap.

In addition, Kwak et al. [28] measured the heat transfer distribution of the squealer tip. The cavity depths were 2.1%, 4.2% and 6.3% of the blade span. The results mentioned that the increase in the cavity depth causes the heat transfer to decrease. When considering the effect of cavity depth and rim width, Zhou [29] discussed the influence of cavity depth and rim width on the aerothermal characteristics of tip. Cavity depth and rim width could affect tip contraction coefficient and change leakage flow. Reducing rim width could constrain TLF. The average tip heat transfer coefficient could be reduced by 12.77% as the cavity depth increased. Park et al. [30] experimentally measured the heat/mass transfer distributions on the squealer tip among different tip clearances and rim heights. The results showed that the high heat transfer on the tip appeared on the suction side rim at x/C_{ax}=0.1, and then the heat transfer on the squealer tip decreased to the trailing edge.

Besides, Sakaoglu and Kahveci [31] studied the effect of tip injection and rotation on the squealer tip. The results showed that the squealer tip enlarged the volume over the tip, and the TLF was restrained inside the cavity, forming a low momentum fluid. The increased cavity depth changed the strength and location of vortices in the squealer tip. The film effectiveness increased with cavity depth increasing for the rotation cases with the addition of cooling.

Bang et al. [32] experimentally studied the effects of unsteady wakes on heat transfer on the squealer tip, and the unsteady wakes made high turbulence intensity of leakage flow and heat/mass-transfer distributions changed. Recently, Senel et al. [33] further refined the vortex system structure in the cavity and pointed out the influence of cavity depth on the aerothermal characteristics in detail. The result showed that the cavity depth increased the cavity volume, which led to enlarge the cavity vortex near PS (PSCV) and the cavity vortex SS (SSCV). The intensive cavity vortex system improved the blockage to TLF. And the backflow regions PSCV and SSCV isolated from the cavity bottom and high momentum leakage jet, resulting in the decrease of heat transport. The averaged Nu_{tip} reduced by about 17.2% as the cavity depth increased from 1% to 2.4%.

To summarize from the above, increasing the cavity depth could affect the cavity volume, which enlarged the cavity vortex structures to constrain the TLF and heat load of the tip. In addition, the usual proportion of cavity depth to blade span is basically kept at about 3%, and the maximum depth studied by Kwak et al. [28] is 6.3%. In view of the above, the conventional cavity depth conventional cavity depth is always below 7% blade span (H). Follow this line of thought, if the cavity depth is significantly increased on this basis, the volume inside

the cavity is conducive to the development of the backflow vortex, but the specific effects on the suppression of the TLF and heat load on the tip are still unknown. Besides, with the increase of cavity depth, the blade mass decreases and the corresponding centrifugal force decreases, which reduces the load on blade tip and helps to improve the service life of the blade. Other than that, the design of the squealer tip with deep scale depth tip in the study is derived from a real turbine blade of a key aero-engine. The thermal load of the turbine blade is not very high, so there is no cooling structure. At the same time, for the key index of weight loss, it is designed as a squealer tip with deep-scale depth. In view of the above, this study aims to explore the influence of squealer tip with deep-scale depth (≥7% blade span) and conventional cavity depth (<7% blade span). Thus, the blade weight can be minimized based on reducing leakage flow and weakening tip heat transfer. In the light of above factors, the research on the squealer tip with deep scale depth in this study is very meaningful, which can not only explore the influence of deep cavity on clearance leakage flow and turbine aerothermal characteristics, but also provide a theoretical basis for the design of a certain engine blade.

2. Numerical Method

2.1 Computation model

The computational domain is a single blade passage, which is similar to the experimental model of Kwak and Han [7, 34]. Fig. 1(a) shows the simulation model of the blade. The blade model is a threefold scaled-up model of the GE-E3 blade. Additional details are available in Timko [35]. Fig. 1(a) shows that a typical HPT blade profile, and the height of tip clearance (τ) is about 1% of blade span (H). The axial chord length of scaled-up blade is 0.0861 m. The inlet flow angle is 32.01°, and the exit angle is 65.7°. The squealer rim width (W) is about 2%H and four cavity depths (d_i) are adopted, d_1, d_2, d_3 and d_4, respectively. Table 1 shows the detailed geometric parameters. Fig. 1(b) shows the tip clearance outlet surface of suction side, which is named as S0. This S0 section is the integral surface used in the following integral calculation of tip clearance leakage mass flow.

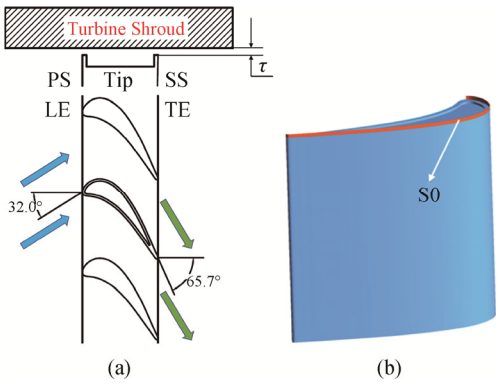

Fig. 1 Sketch of computation model and geometric parameters. (a) Turbine blade geometry (b) Definition of the suction side tip clearance outlet surface

In this study, different cases such as a flat tip (FT), and a squealer tip with cavity depths of 1%H (STd_1), 3%H (STd_2), 10%H (STd_3) and 30%H (STd_4), are considered. The tip clearance heights with 1%H, 1.5%H and 2.5%H are defined as G1, G2 and G3. Fig. 2 shows the definitions of the different tip configurations.

Table 1 Geometric parameters of blade

Parameter	value
Axial chord, C_{ax}	86.1 mm
Span, H	122 mm
Blade spacing	91.5 mm
Aspect ratio	1.4
Tip clearance height, τ	1%H–2.5%H
Squealer depth, d_1–d_4	1%H–30%H
Squealer width, W	2.29 mm

2.2 Computation domain and Boundary conditions

Fig. 3 displays the computation domain linear cascade passage. The inlet is placed approximately at 1C_{ax} upstream of LE. The distance between the exit and outlet sections is set to 1.8C_{ax} length, which allows the downstream flow to be fully developed. The exit is set as an average static pressure boundary condition. On the blade and shroud wall boundaries, the temperature is set to 340 K. The airflow temperature used in the calculation is not the high temperature of the engine under the real working condition.

On the one hand, such calculation conditions are modeled from real engine conditions, and on the other hand, they are used to guide the experimental design and verification in subsequent experimental studies. Moreover, adiabatic non-slip boundary conditions are applied to below the endwall of the channel. Period boundary condition is set on the two sides of the passage. The specified information is shown in Table 2. The exit velocity of cascade channel is 199 m/s and Mach number at the exit of the channel is 0.59. The Reynolds number calculated from the axial chord length of the blade and cascade outlet velocity is 1.1×10^6. The above boundary parameters are consistent with the experimental tests [7, 34] and are used as the boundary conditions for the numerical calculation in this study.

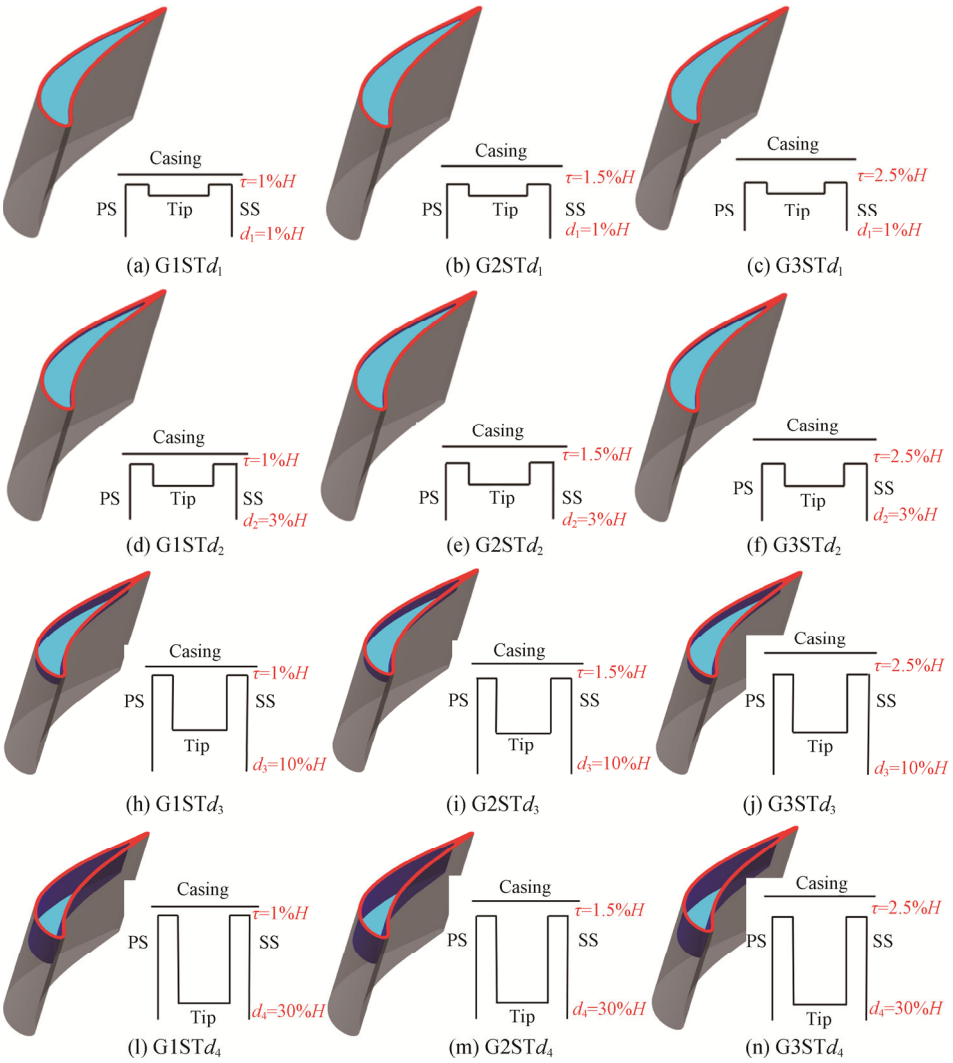

Fig. 2 Schematic of different tip configurations

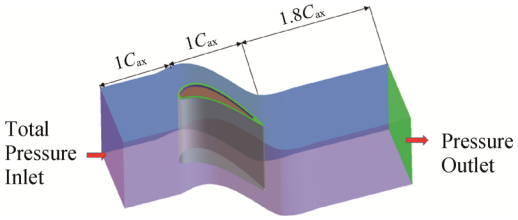

Fig. 3 Computational domain

Table 2 Boundary value settings

Boundary	Boundary condition	Value
Inlet	Inlet total temperature/K	297
	Inlet total pressure/kPa	126.9
	Turbulence Intensity/%	9.7
	Turbulence length scale/cm	1.5
Outlet	Exit static pressure/kPa	102.7
	Exit Mach number	0.59
Wall	Wall temperature/K	340

2.3 Computational mesh

In this study, a structured mesh was generated by Numeca Autogrid5. In order to make the grid to meet the needs of computing, the H-type grid topology was used for cascade, and an O-type grid topology was adopted around the blade surface and tip clearance. Local refined was carried out near LE, TE and squealer rim. The growth rate of was set to 1.2, and the thickness of the first layer meshes near the wall was 0.001 mm. The y^+ is not greater than 3, which can meet the needs of the selected turbulence model. Fig. 4 displays the global grid and local grid of squealer tip.

2.4 Defined parameters

The static pressure loss coefficient (C_p) is defined as follows:

$$C_p = \frac{P_{t,in} - P}{P_{t,in} - P_{out}} \tag{1}$$

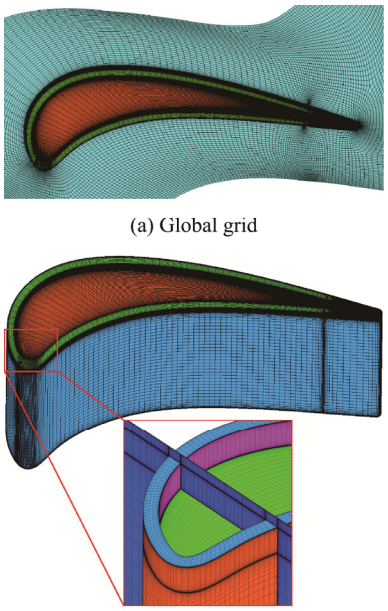

(a) Global grid

(b) Grid of Squealer tip

Fig. 4 Computational mesh

where P is the local pressure; $P_{t,in}$ is the averaged total pressure of the inlet, and P_{out} is the averaged static pressure of the exit.

The heat transfer coefficient is the ratio of wall heat flux and the temperature difference between the qualitative temperature and the local wall temperature:

$$h = \frac{q_w}{T_w - T_{ad}} \tag{2}$$

where q_w is the wall heat flux; T_w is the solid wall temperature, and T_{ad} is the adiabatic temperature near the wall.

The area-averaged heat transfer coefficients h_{ave} is defined as follows:

$$h_{ave} = \int h \mathrm{d}A \Big/ A \tag{3}$$

where A is the area of the tip surface.

The Nusselt number is defined as follows:

$$Nu = h\delta/\lambda \tag{4}$$

where δ is the characteristic length, which is the chord of the current model, and λ is the thermal conductivity of the gas.

Heat duty is the heat flow into the area at the tip.

$$Q = \int_A q \cdot \mathrm{d}A \tag{5}$$

where A is the area of the tip surface.

To explore the variation in the leakage flow, the relative leakage mass flow rate is investigated. The leakage flow mass at S0 is denoted m_{leak}. Thus, the ratio of tip leakage mass flow (m_{leak}) to main mass flow (m_m) is called the relative leakage mass flow rate, which is defined as follows:

$$\varepsilon = \left(m_{leak}/m_m\right) \times 100\% \tag{6}$$

To quantitatively analyze the "irreversible equilibrium process" of the mixing flow, the entropy production rate is proposed in the paper [34], which is defined as follows:

$$S_1''' = \frac{2\left(\mu + \mu_T\right)\overline{s}_{i,j}\overline{s}_{i,j}}{\overline{T}} + \frac{\left(\lambda + \lambda_T\right)}{\overline{T}^2}\frac{\partial \overline{T}}{\partial x_i}\frac{\partial \overline{T}}{\partial x_i} \tag{7}$$

where the μ_T is turbulent viscosity coefficient; λ_T is turbulent heat transfer coefficient and $\overline{s}_{ij}$ is the strain rate tensor. The right side of formula consists of two entropy production, which is respectively derived from the effect of viscosity and heat transfer. The detailed loss mechanism of leakage flow could be measured by investigating the entropy production rate, which is caused by viscosity and heat transfer.

2.5 Grid-dependence

To prevent the lack of mesh density from affecting the accuracy of the calculation results, the meshes used in this study increase the nodes of meshes in tip clearance region and near cavity, and then we analyzed its mesh independence. Five cases of squealer tips with different clearance spreading grid densities were calculated respectively as shown in Table 3. The number of grid nodes in the clearance increased from 20 to 30, 35, 40 and 45 layers in turn. In addition, the streamwise, pitch direction and spanwise of cascade passage were all verified by the number of grid nodes, and especially it contained the validation of the number of nodes in the cavity in the direction of depth. Fig. 5 shows the proportion of leakage in the flow of the main channel, the average heat transfer coefficient and the pressure ratio along with the blade profile at 98% of the axial direction of the blade, as calculated by five different grid numerical examples.

It can be seen that, with the increase of mesh number, tip leakage and average tip heat transfer coefficient decrease gradually. And the blade profile pressure ratio at 98% of the span decreases firstly and then increases gradually with the quantity of mesh increasing. When the number of grids in the clearance is more than 40, the change of leakage quantity (the ratio of leakage quantity to the total leakage quantity) is less than 0.05%, and the change of blade profile pressure ratio at 98% of the span is less than 0.01%. It can be considered that the leakage

Table 3 Cases of varied mesh allocation

	Streamwise×Pitch×Spanwise(Gap)×Depth	Total Number/10^6
Grid 1	115×71×135(20)×9	2.17
Grid 2	133×81×150(30)×17	2.98
Grid 3	151×85×155(35)×17	3.53
Grid 4	169×101×180(40)×33	5.04
Grid 5	187×101×195(45)×38	5.91

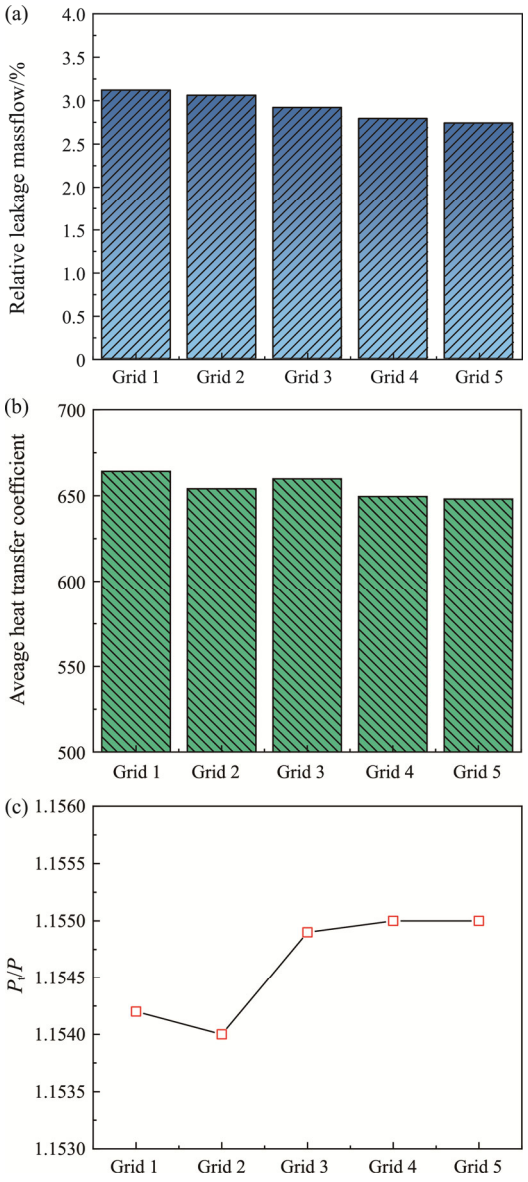

Fig. 5 Mesh independence validation. (a) Relative leakage mass flow rate, (b) the average heat transfer coefficient of tip, (c) pressure ratio of blade profile at 98% spanwise

performance, tip heat transfer features and aerodynamic potency do not change. Therefore, the grid strategy with 40 grid nodes across the clearance direction can meet the requirements of numerical calculation accuracy for turbine aerodynamic performance and heat transfer characteristics. That is, Grid 4 can satisfy grid independence.

2.6 Numerical methods and validations

The numerical simulation displayed in this study was conducted by ANSYS-CFX. The results were calculated by figuring out the steady-state Reynolds Averaged Navier-Stokes equations. The fluid is assumed to behave as an ideal gas. The governing equations contain continuity equation, momentum equations and energy equation, which are calculated by adopting the method of finite volume. And the high resolution scheme is used for discretization. The convergence criterion is that the root mean square residuals of above equations are calculated to reach the levels of 10^{-4}–10^{-5}. To obtain more reliable of numerical calculation, the standard k-ω turbulence model was selected to verify the accuracy of the CFD methods.

The verification was performed by comparing numerical results and experimental data of a flat tip, and the height of tip gap is 1% of the blade height. The experimental test was conducted on a five-blade linear cascade. The inlet total pressure was 126 kPa and the overall pressure ratio was 1.23. Detailed flow conditions were described concretely in the experimental introductions [8, 34]. On basis of the experimental model and working conditions, the three-dimensional numerical simulation was carried out. Fig. 6 plots the pressure distribution and heat transfer of the experimental data [8, 34] and the predicted value-form in this paper. Fig. 6(a)–6(d) show the pressure distribution at 50%, 80%, 90% and 97% of the blade span; the ratio of total inlet pressure to local static pressure (P_t/P_s) on the PS is close to the experimental result. In general, the pressure distribution data predicts the experimental data very well. The simulation data of SS is close to the experiment result at the LE and TE, and the ratio of SS at the mid-chord region is a little bigger than the experiment result. However, the data solved by using stand k-ω turbulent model is closer to the experimental value among three turbulent models. Besides, Fig. 6(e) shows that k-ω turbulence model is closer to the experimental value than SST model and SA model in terms of the overall trend of the tip heat transfer. Fig. 6(f) showed the averaged heat transfer coefficient of experimental result and numerical results at pitch direction on blade tip. The averaged heat transfer coefficient on the tip shows a trend of decreasing from high value at leading edge, then gradually increasing, and then decreasing to trailing edge. Three turbulent models could well predict the distribution of heat transfer coefficient at blade tip, and stand k-ω turbulent model performs better SST model and SA model in the comparison with pitch-averaged h on the tip. Combined with the research on the squealer tip to be carried out below, the comparison between the experimental results [37] and the calculated results [38] in the literature is also presented to verify the rationality of the k-ω turbulence model. Fig. 6(g) showed the same region of high heat transfer, such as regions A and B. In addition, the calculated pitch-averaged heat transfer coefficient is similar to the plot in the study [38], and the numerical results are both bigger than the experimental

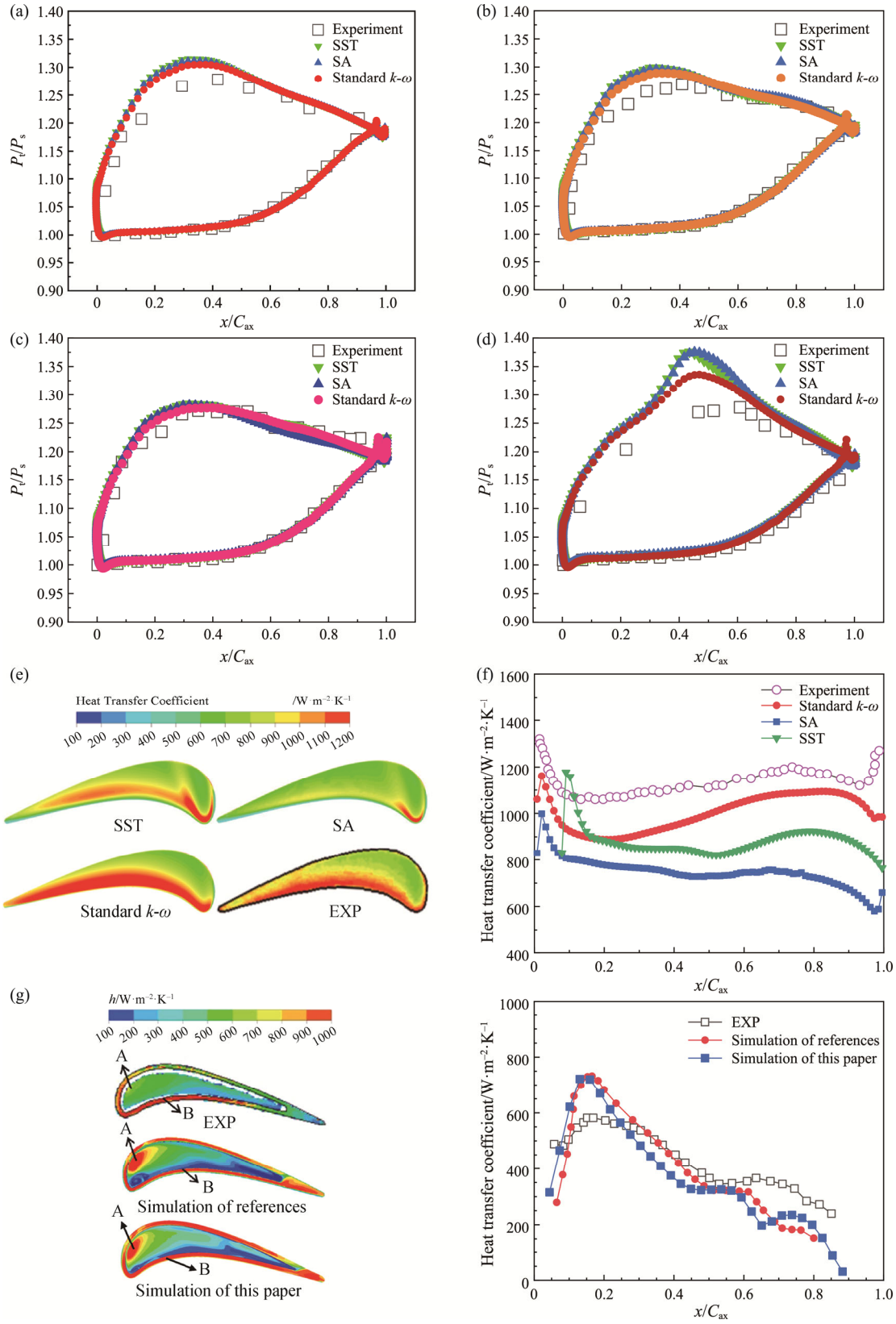

Fig. 6 Validation between the numerical results and experiment data. (a) Pressure distribution at midspan, (b) Pressure distribution at 80%span, (c) Pressure distribution at 90%span, (d) Pressure distribution at 97%span, (e) The numerical heat transfer coefficient on flat tip and experiment result [8, 32], (f) Comparison of pitch-averaged heat transfer coefficient on flat tip with experimental value [8, 32], (g) Comparison of CFD results on squealer tip with experimental value [35, 36]

results on the floor near the LE, but the overall trend is the same. Moreover, previous investigations about tip leakage flow, such as those of Yan et al. [21], Du et.al [23], Jiang et al. [24], Ye et al. [38], Ameri et al. [39], Yang and Feng [40], He [41], and Li et al. [42] also showed that the k-ω model could verify the experimental results. From what has been discussed above, the turbulence model used in the calculation of this study is standard k-ω turbulence model.

3. Results

3.1 Leakage flow characteristics under large scale deep cavity

Based on the above validations, numerical calculation is conducted to investigate the effect of a deep-scale cavity. To study the influence of deep-scale cavity on leakage flow characteristics, four cases with a cavity depth of 1%H, 3%H, 10%H and 30%H were analyzed and compared, respectively.

Fig. 7(a) shows the C_p on a middle cut plane of tip gap. The C_p is large near the PS and SS, which is due to the inlet effect and outlet effect of leakage flow. The pressure coefficient near PS is significantly reduced as cavity depth increases. As the cavity depth deepens to 3%d, the C_p of the circular region I in the black dotted line is more significant than that of other areas on PS. The remaining C_p near PS is significantly reduced. This means the static pressure at most of the area near the PS increases, which could effectively block the leakage flow. In addition, the region II decreases obviously, but the C_p in region IV is slightly increased as the cavity depth enhances from 10%H to 30%H. This will result in reduced containment of the leakage flow.

Fig. 7(b) displays Mach number distribution on the tip gap. Fig. 7(b) shows that Ma at tip gap is higher at SS near LE and PS. For the LE region of black rectangular dotted box near PS, the area of high Ma shows a trend of increasing first and then decreasing with cavity depth increasing, as shown at the regions A1–A4. This means the velocity of leakage flow increases first and then decreases with cavity increasing. For the PS region of the black rectangular dotted box, the region i of high Ma is distributed at the corresponding position of separation zone at the inlet of a gap. The part ii decreases to a narrow strip region when the cavity depth deepens to 3%H. As the depth enhances substantially to 10%H, the high Ma region of region iii disappears in the middle and posterior part of the pressure side. However, when the cavity depth increases to 30%H, the high Ma of region IV increases and then returns to the strip distribution. Overall, the high Ma region at the PS decreases first and then increases slightly with the cavity depth increases, which means that the inhibition of leakage flow in most areas of the PS increases first and then increases somewhat as cavity depth increases.

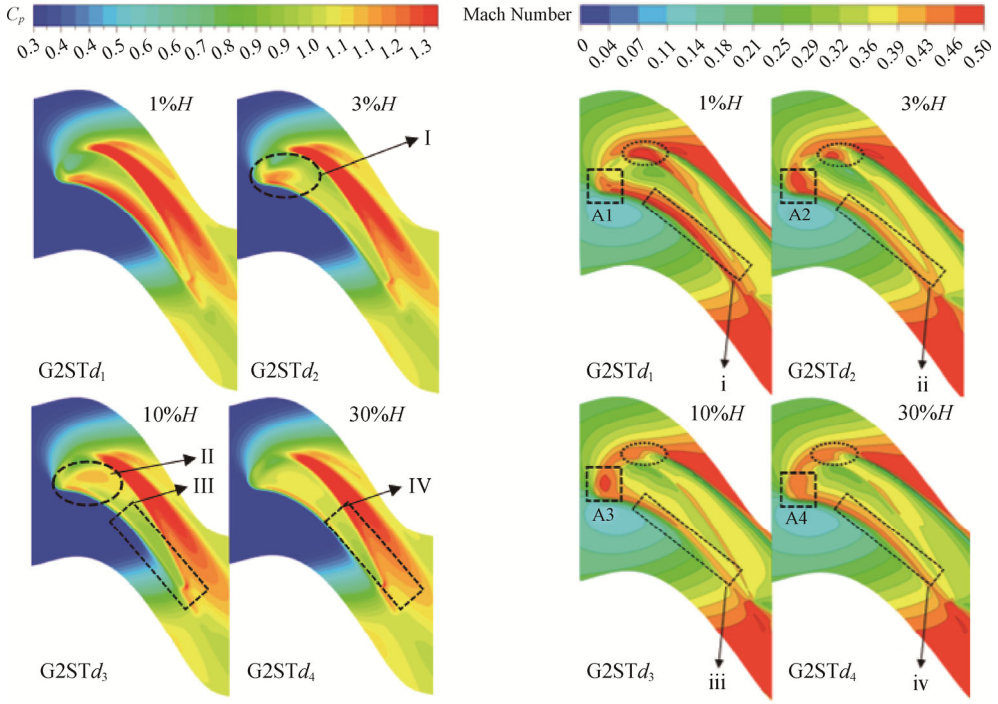

(a) Static pressure coefficient (b) Mach number

Fig. 7 The flow parameters distribution on the tip gap

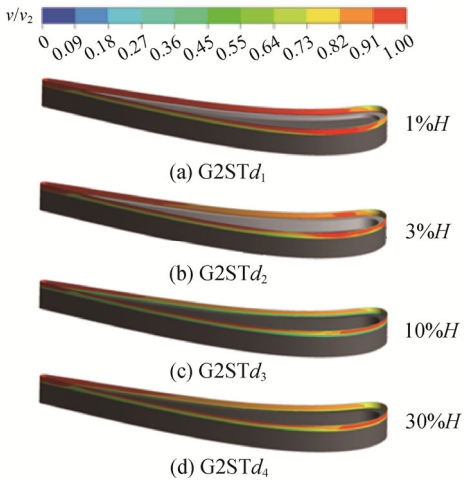

Fig. 8 Dimensionless velocity distribution of tip gap

The above is the overall distribution of the leakage flow in the passage, and the change of the leakage flow can be intuitively seen from the velocity distribution at tip gap. Fig. 8 shows the comparison of dimensionless velocity of gap inlet and outlet sections, and v_2 is the isentropic velocity at cascade outlet, and v/v_2 can compare the change of leakage flow velocity caused by the increase of cavity depth. Fig. 8(a) shows that v/v_2 of tip gap at PS and SS are basically above 0.9, and only about 0.6 on the SS near the tip region. The v/v_2 reduces obviously as the cavity depth increases from 1%H to 10%H; the v/v_2 of G2STd_3 decreases to about 0.55 below half gap. However, the v/v_2 increases as the cavity depth continues to increase to 30%H. In general, the v/v_2 at the tip gap first decreases and then grows with the cavity depth increasing.

Fig. 9(a) shows the relative leakage mass flow rate (ε) at different cavity depths. As the cavity depth increases from 10%H to 30%H, the ε gradually increases from 2.3% to 2.6%. This is consistent with the variation of velocity distribution with cavity depth increasing in the Fig. 8. The ε of G2STd_3 reduces by 20.6% in contrast to G2STd_1.

To further analyze the effect of cavity depth on the leakage flow development, the mass distribution per unit area of leakage flow (m_{ave}) along the suction side outlet section was compared. Fig. 9(b) shows the m_{ave} of G2STd_1 and G2STd_2 both reach the maximum at $0.3C_{ax}$. The increase of cavity depth has a significant effect on the range of $0.1C_{ax}$–$0.6C_{ax}$ under conventional cavity depth.

When the depth of the cavity increases to the deep-scale, the maximum m_{ave} at the clearance outlet of G2STd_3 is around $0.6C_{ax}$. As the cavity depth increases to 30%H, the m_{ave} of G2STd_4 is higher than that of G2STd_3 after $0.1C_{ax}$. Generally speaking, the m_{ave} decreases significantly between $0.1C_{ax}$ and $0.6C_{ax}$ with cavity depth

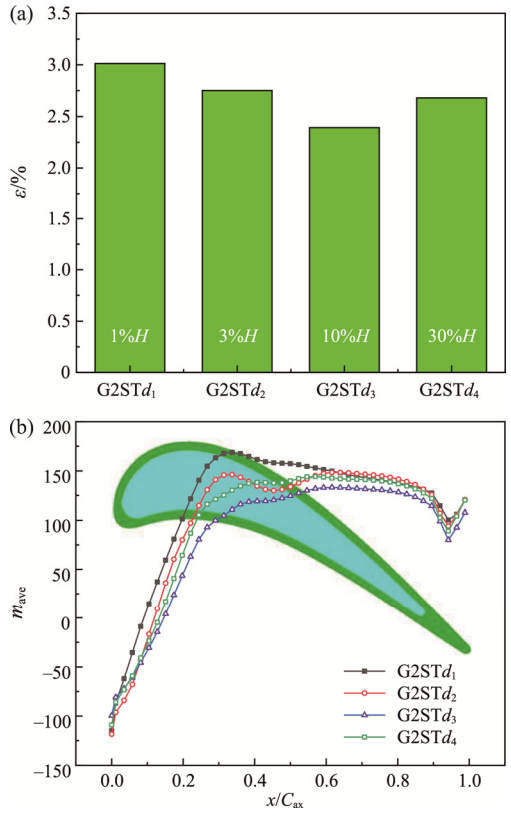

Fig. 9 Leakage flow parameters at different cavity depth. (a) Relative leakage mass flow rate, (b) Distribution of leakage flow along streamwise

increasing in the range of traditional depth. That means the inhibition effect on leakage is diminished in the middle to the rear of the cavity. With the increase of cavity depth in the range of deep-scale, the relative leakage rate tends to increase on the whole.

To analyze the development process of leakage flow in the cavity and channel, the leakage flow distribution at different axial positions is compared. Fig. 10(a) displays the schematic diagram of the section perpendicular to the mean camber line at different axial positions. The three sections are defined as S1, S2 and S3, respectively.

Fig. 10(b) shows the streamlines and dimensionless velocities at S1 section. The leakage flow forms a cavity vortex in the cavity near the PS and then a leakage vortex is formed near SS. The velocity in the leakage vortex region a1 is large, and the v/v_2 is above 0.9. The cavity vortex inside the cavity enlarges and the v/v_2 of region a2 decreases to about 0.8 with the cavity depth increasing. As the cavity depth is increased from conventional depth to deep-scale, the space of the cavity increases, which makes the cavity vortex fully develops. Fig. 10(b) shows the velocity of cavity reduces obviously and the v/v_2 of region a3 decreases to 0.7. The larger cavity on the tip causes the cavity vortex to develop into two large vortexes. The dimensionless velocity in most areas of the

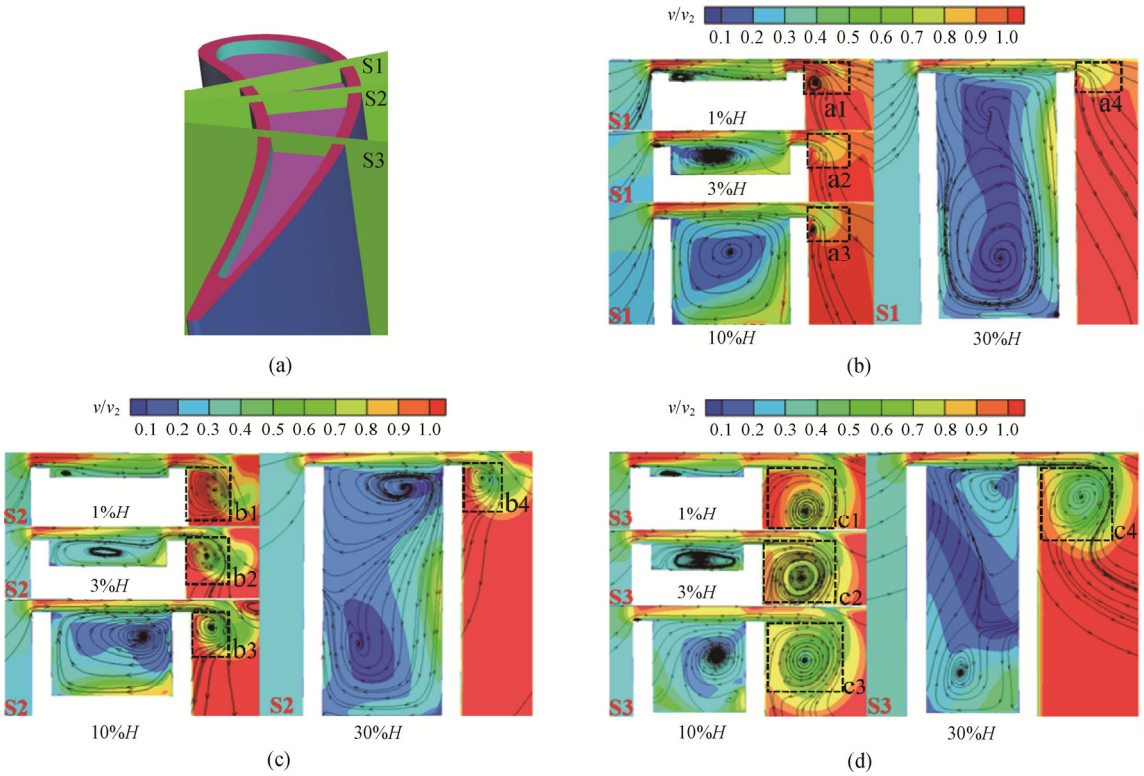

Fig. 10 Streamline and dimensionless velocity at different axial positions. (a) Diagram of sections at different axial positions, (b) S1 section, (c) S2 section, (d) S3 section

cavity reduces to 0.1. Furthermore, the center of the cavity vortex gradually moves from PS to SS with cavity depth increasing. The vortex core of G2STd_3 is basically in the mean camber line of the cavity.

On the S2 section, as shown in Fig. 10(c), the vortex core of G2STd_3 moves towards the SS and the velocity at the region of leakage vortex (b1–b4) decreases obviously. For the section S3 at the middle and rear area of the tip, the width of cavity decreases, which leads to the decrease of cavity vortex, as shown in Fig. 10(d) 10%H. And Fig. 10(d) shows the v/v_2 in the leakage vortex region from c1 to c3 gradually decreases to 0.6, while the dimensionless velocity of c4 region increases to 0.9. In a nutshell, the cavity with deep-scale depth could provide enough volume to accommodate the development of vortex systems, and the cavity vortex diminishes the velocity in the cavity and gap. However, the excessive cavity depth divides cavity vortex into two and reduces the velocity of cavity vortex, which increases the velocity of leakage vortex. The influence of the vortex system in the cavity on the flow in the gap still needs to be further analyzed.

After the flow distribution in the cavity is analyzed, the loss intensity in the cavity also needs to be characterized. Fig. 11(a) shows the cut plane at the 20%C_{ax} location. The cross-section in the red dotted box is the cut plane below the tip, representing the part in the cavity. And the green section on the upper side represents the part inside the tip gap. Fig. 11(b) shows the distribution of entropy production rate (EPR) at the location of 20%C_{ax}. The high EPR distributes on the inlet and outlet of clearance, and the region of high EPR increases obviously with the cavity depth increasing from 1%H to 3%H, such as region A and B. The high EPR at the region of leakage flow vortex reduces with cavity depth increasing. Thus, the increase of cavity depth enlarges the strength of flow mixing, which reinforces the suppression of the leakage flow.

When the cavity depth increases to a deep-scale, the velocity inside the cavity decreases, which changes the overall flow mixing in the cavity. As the cavity depth increases by 10%H, the uniformity of the high EPR region decreases, and the region of high EPR is transitioned to the floor and rim wall near the SS. In addition, the EPR at the most parts inside the cavity is not high. However, the cavity volume enlarges with depth increasing, so it is not sure whether the total entropy production rate on the cut section increases or decreases. This needs to be analyzed from a quantitative point of view.

Fig. 11(c) shows the dimensionless entropy production rate (DEPR) on the cut plane. The dimensionless value is the ratio of the total value of EPR to the case with 10%H depth. The overall DEPR first increases and then decreases with the cavity depth increasing, which obtains a maximum increase of 43.54% compared to G2STd_1 as the cavity depth is 10%H. Besides, the DEPR inside the

cavity only also has the same law of change, which increases by 135% in contrast to G2STd_1 as the cavity depth is 10%H. This means that the leakage loss inside the cavity is the biggest as the cavity depth is 10%H. The cavity depth changes the strength of flow mixing inside the cavity. As Zeng et al. [11] and Zou et al. [18] mentioned, tip leakage loss contains inter gap loss and loss outside the gap, and the most of leakage loss is due to the mixing of leakage flow and main flow outside the gap. The total leakage flow loss is obtained by comparing the loss in the channel with and without clearance. In this way, the proportion of mixing loss to leakage loss is calculated; the values of proportion are 87.5%, 81.6%, 78.1% and 80.2% when the cavity depth increases from 1%H to 30%H, which is consistent with the trend of leakage flow with changing depth.

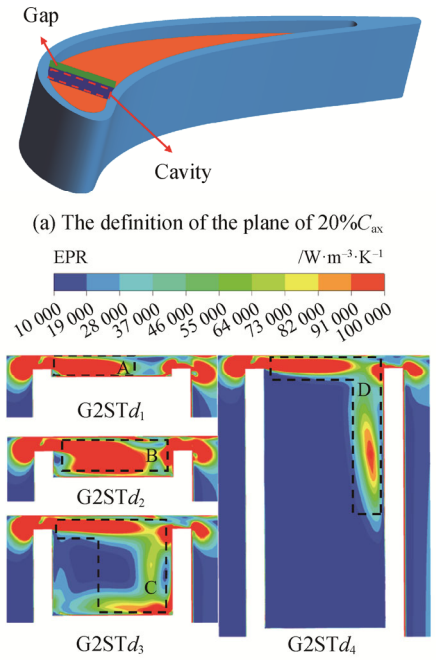

(a) The definition of the plane of 20%C_{ax}

(b) Comparison of entropy production rate at different cavity depth

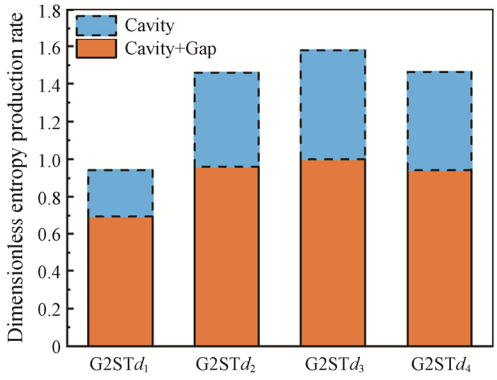

(c) The dimensionless entropy production rate on the cut plane

Fig. 11 Entropy production rate distribution on the cut plane of 20%C_{ax}

3.2 Heat transfer characteristics under large scale deep cavity

The cavity depth is developed from conventional scale to the deep-scale, which affects the development of TLF as above. Meanwhile, the heat transfer characteristics of tip are also affected. Fig. 12 displays the heat transfer coefficient of tip and rim surface at four cavity depths. The heat transfer distribution of rim top at PS and SS is larger as the cavity depth is 1%H. This is due to the import effect of the leakage flow entering the gap, and the accelerating outflow of the decreasing channel from the SS, as shown in Fig. 10. The most obvious one is that in the region A of the cavity near LE, due to the leakage flow rushes to the bottom of the cavity, a cavity vortex is formed, and a local high heat transfer coefficient region is generated. Deeper cavity depth enhances vortex size, and the vortex core moves to SS, forming the high heat transfer region B as Fig. 12(a). As a result of heat transfer distribution of conventional squealer tip, which is consistent with the view that the region of high heat transfer on the tip was formed at the leading edge near the suction side, and then decreased until to the trailing edge in the study reported by Park et al. [28].

When the cavity significantly increases to 10%H, Fig. 10 shows that the cavity floor is far away from the gap leading to an enhancement in the volume of the cavity, resulting in a more enormous cavity vortex with low velocity covering the bottom, which reduces the impact effect of the leakage flow on the cavity bottom, thus weakening the convective heat transfer intensity and forming a small high heat transfer region C as Fig.12(a). As the cavity depth increases to 30%H, there are two upper and lower reflux vortexes in the cavity. The impact of the leakage flow on the cavity bottom is further cut off, as shown in Fig. 10. The high heat transfer region disappears, and the heat transfer coefficient of the region D decreases.

Fig. 12(b) shows the heat transfer coefficient of the rim surface at four cavity depths. The high h on the rim surface of SS decreases at the direction of the chord with the cavity depth increasing. The local high h is mainly focused on the rim surface of SS near LE when the cavity depth is 30%H. This is because the TLF that enters gap impinges the region and results in high h. Due to the impact velocity decreases with the cavity depth increasing, as shown in Fig. 10.

Fig. 13 shows the average heat transfer coefficient of the pitch direction at the cavity bottom along the axial chord. The h_{ave} increases first and then decreases along the axial direction. However, the position of the maximum value gradually moved to the trailing edge with the cavity depth increasing. The location of the maximum value occurs in turn at 0.08C_{ax}, 0.12C_{ax}, 0.23C_{ax} and 0.57C_{ax}. The change range of the overall h_{ave} of G2STd_4 is smaller than that of the other three cavity depths.

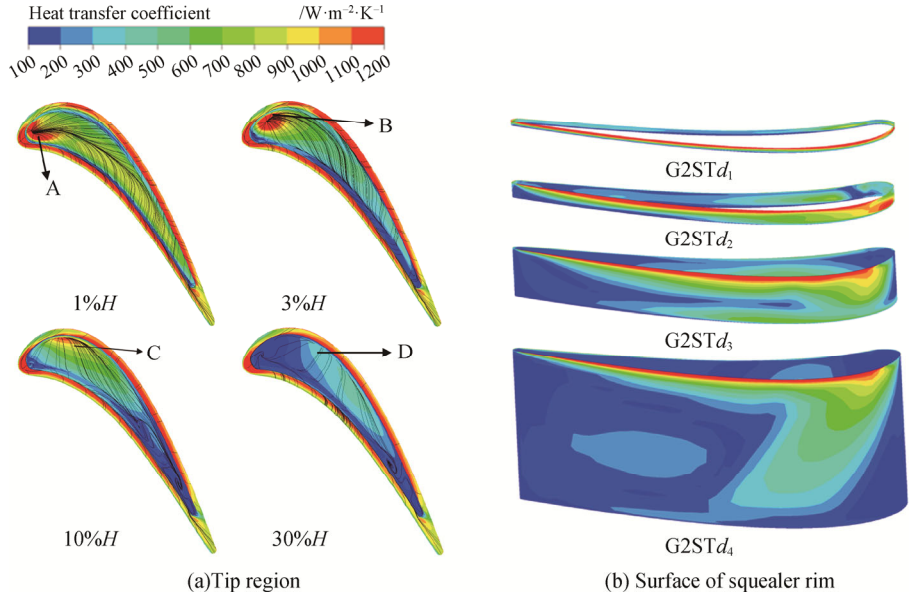

(a)Tip region (b) Surface of squealer rim

Fig. 12 Heat transfer coefficient at different cavity depth

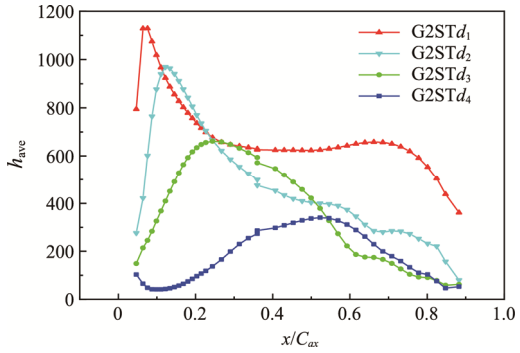

Fig. 13 Average heat transfer coefficient of the pitch direction at cavity bottom along the axial chord

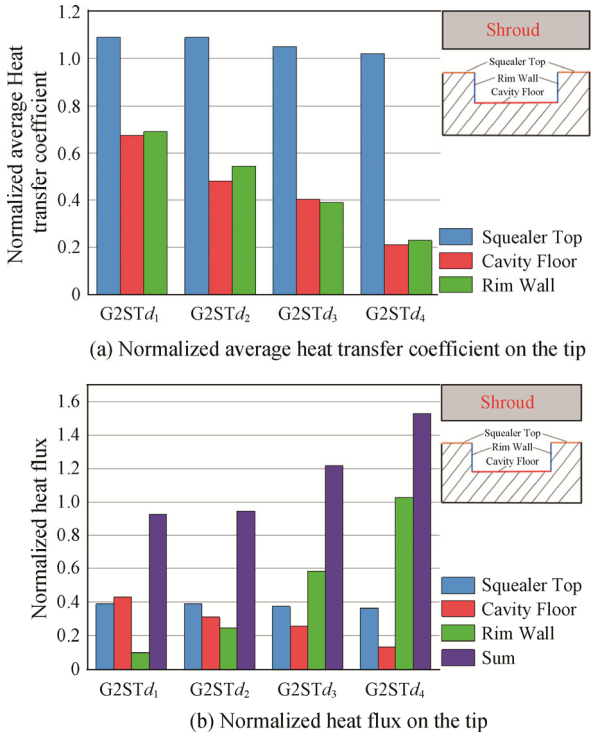

(a) Normalized average heat transfer coefficient on the tip

(b) Normalized heat flux on the tip

Fig. 14 Heat transfer characteristics of blade tip

Fig. 14 shows the normalized average heat transfer coefficient and normalized heat flux at a different area of squealer tips. These normalization reference values are the result of flat tips at a tip clearance of 1%H. For all squealer tips with different depths, the highest h appears on the squealer top. As the cavity depth increases, the h reduces on the squealer top, rim wall and cavity floor. The normalized average heat transfer coefficient of the squealer floor reduces by about 28.17% when the cavity depth increases from 1%H to 3%H, and the corresponding reduction for the squealer top and the rim wall are respectively –0.011% and 20.97%. The corresponding reduction of G2STd_3 for the squealer floor, squealer top and rim wall are respectively 40.26%, 3.58% and 76.89%, in contrast to the cavity depth of 1%H. As the cavity depth increases from 10%H to 30%H, the corresponding reduction for the squealer floor, squealer top and the rim wall are respectively 47.56%, 2.27% and 41.37%. Therefore, the heat transfer coefficients on the bottom and rim can be significantly reduced by increasing the depth of the cavity at both conventional and deep-scale depths.

Fig. 14(a) shows that the deepest squealer tip obtains the lowest normalized average heat transfer coefficient. Nevertheless, deeper cavity enhances the surface of the cavity. Fig. 14(b) shows the heat flux of different cases. The total heat load of G2STd_4 is 25.45% higher than the G2STd_3 and 65.14% higher than the G2STd_1. The

thermal loads in different areas of the tip are divided. The heat load of G2STd_4 on the rim reached the highest among the four squealer tips. Whereas, appropriate heat distribution can be obtained by reasonable cooling methods such as tip cooling.

The two parts of the squealer top and cavity floor are essential components of the tip. The heat load and h on the squealer top barely changes with cavity depth increasing. For cavity floor, the h and heat load obviously decrease with cavity depth increasing. Thus, the heat load and h of the blade tip could be effectively weakened as cavity depth increases. The increase of total heat load is due to the increase of the rim surface, and it can be effectively reduced by reducing the local region of high heat transfer coefficient. Therefore, the most important thing is to effectively reduce heat transfer coefficient and heat load of the squealer top. Combined with the above analysis, based on selecting appropriate deep-scale cavity depth, the cooling design which can effectively reduce the squealer top should be added, such as internal cooling, winglet tip and cavity separator.

3.3 Aerothermal characteristics of deep-scale cavity varying with tip clearances

To study the aerodynamic characteristics of the deep-scale cavity in different blade tip clearances, the relative leakage mass flow rate (ε) on different clearance height (τ) is compared. Fig. 15 shows that the ε obviously increases with tip clearance increasing. As the clearance is 1%H, the ε enhances first and then declines with the maximum decrease of 21.48% with cavity depth increasing. When the tip clearance increases to 1.5%H and 2.5%H, the ε decreases first and then increases with the maximum decline of 11.08% and 13.67%, respectively. Deep-scale cavity is more effective in inhibiting leakage flow at smaller tip clearance.

Fig. 16 displays the normalized average h at three different tip clearances. These normalization reference average heat transfer coefficients are the result of flat tips at a tip clearance of 1%H. For all tip clearances, the squealer top presents the highest h among three components. As the τ is 1%H, the normalized average h of squealer floor reduces at most by about 72.6% with cavity depth increasing. The corresponding reduction of rim wall and squealer top are 69.37% and 5.78%, respectively, in contrast to the case with cavity depth of 1%H. As the tip clearance height is 1.5%H, the corresponding maximum reduction of cavity floor, rim wall and squealer top are 68.67%, 66.85% and 6.25%, respectively with cavity depth increasing. When the tip clearance increases to 2.5%H, the corresponding maximum reduction of cavity floor, rim wall and squealer top are 49.45%, 60.73% and 4%, respectively with cavity depth increasing.

In general, the enlarged gap diminishes the declining quantity of normalized average h. The clearance height has little effect on the squealer top, but has a noticeable effect on the rim wall and cavity floor. For the tight clearance, deep-scale cavity depth performances better on reducing the average h of the blade tip.

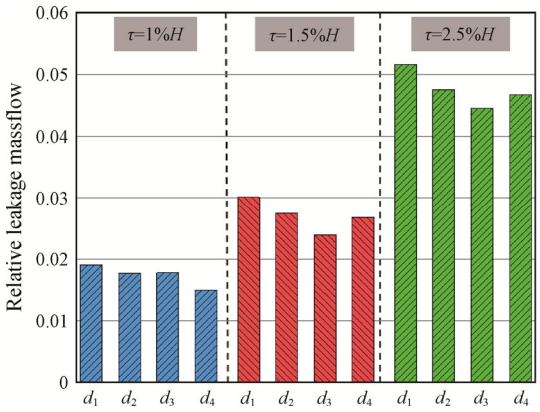

Fig. 15 Relative leakage mass flow for three tip clearance height

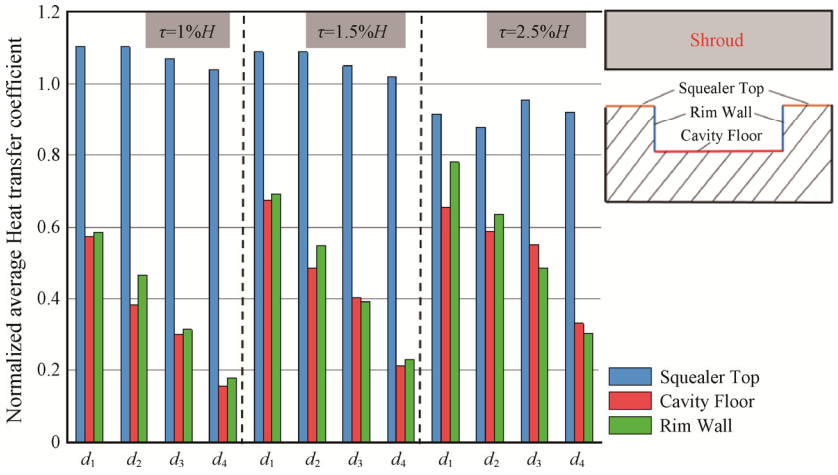

Fig. 16 Normalized average h on the tip for different tip clearance

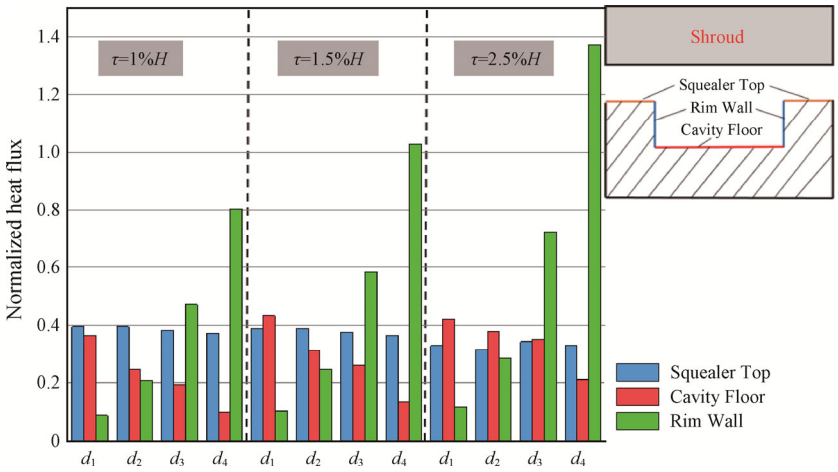

Fig. 17 Normalized heat flux on the tip for three tip clearance

Fig. 17 shows normalized heat flux at three different tip clearances. The normalization reference heat flux is the result of flat tips at a tip clearance of 1%H. The ample tip clearance allows more leakage flow, so that the heat transfer of the tip is affected. The heat load on the squealer top is not sensitive to tip clearance height and cavity depth. The normalized heat flux of the squealer floor reduces respectively at most by 72.6%, 68.67% and 49.45% with the cavity depth increasing when tip clearance is 1%H, 1.5%H and 2.5%H. The corresponding increments for the rim wall are all large for three tip clearances, which all exceeding 800%.

As the cavity depth increases from 1%H to 30%H, the overall normalized heat flux increases by 50.5%, 65.13% and 121% respectively with tip clearance increasing from 1%H to 2.5%H. The deep-scale cavity performances better on reducing heat flux of blade tip. Although the deep-scale cavity could reduce the heat flux of cavity floor, it increases the heat flux of rim wall, so the overall heat flux of blade tip increases.

As the cavity depth increases from 1%H to 3%H, the growth rate of overall heat flux is 0.27%, 2.13% and 12.8% for three tip clearances. Compared with the growth rate of 1%H gap, the growth rate of 1.5%H increases 680%; compared with the growth rate of 1.5%H gap, the growth rate of 2.5%H gap increases 500%. For the deep-scale cavity, when the cavity depth increases from 10%H to 30%H, the increment of overall heat flux is 21.78%, 25.45% and 35.15% for three tip clearances. In hence, the total heat flux of the three different tip clearances is sensitive to the depth variation of deep-scale cavity, but the total heat flux of deep-scale cavity is still higher than that of the traditional depth. In addition, compared with the growth rate of 1%H gap, the growth rate of 1.5%H increases 16.85%; compared with the growth rate of 1.5%H gap, the growth rate of 2.5%H gap increases 27.59%, and they are all obviously smaller than the corresponding growth rate under conventional cavity depth variation. Thus, when the cavity depth increases, the total heat flux of deep-scale cavity is less sensitive to the gap variation.

In general, the deep-scale cavity is suitable for turbines with low gas-thermal parameters, tight tip clearance and large frequency fluctuations of the clearance. For the turbines with high gas-thermal parameters, the heat flux of the blade is so large that it can not be neglected. In the pursuit of low heat load, a cavity with conventional depth has better applicability at various clearance heights. The squealer tip with deep-scale depth is more suitable for small aircraft engines with low power, such as the turboshaft engine.

4. Conclusions

Numerical methods were validated and then used to explore the aero-thermal characteristics of squealer tips with deep-scale cavity depth. The influence of enlarged cavity depth and tip clearance height was also considered. The major outcome of the study is listed as follows:

(1) With the increase of cavity depth at the range of traditional cavity depth, the ε decreases significantly at $0.1C_{ax}$–$0.6C_{ax}$. As the cavity depth enhances based on deep-scale depth, the relative leakage increases as a whole. The distribution of the relative leakage mass flow rate under the deep-scale depth is relatively stable at $0.3C_{ax}$–$0.8C_{ax}$. The dimensionless velocity at the gap outlet section obviously reduces with the cavity depth increasing. In addition, the relative leakage mass flow rate reduces by 20.6% as the cavity depth enhances from 1% to 10%.

(2) For the squealer tip with conventional cavity depth, the leakage flow into the cavity and the cavity bottom near PS appears a reflux vortex. The deepened cavity depth enlarges the size of the reflux vortex. When the

cavity depth increases to 30%H, the larger volume in the cavity causes the cavity vortex to develop from a single vortex into two large vortexes in the upper and lower directions. In addition, the squealer tip with deepened cavity depth causes the center of the reflux vortex gradually to move to SS. When the depth increases to 10%H, the vortex core is basically in the camber line of the cavity.

(3) With the cavity depth developing into a deep-scale, the velocity and uniformity of high entropy production rate (EPR) inside the cavity reduce obviously. However, the increase of depth leads to enlargement of cavity volume, which increases the total entropy production rate as the cavity depth is 10%H. The overall dimensionless entropy production rate (DEPR) of gap and cavity obtains a maximum increase of 43.54% compared to G2STd_1 as the cavity depth is 10%H.

(4) As the cavity significantly increases to 10%H, the enhanced cavity volume results in a more enormous cavity vortex with low velocity covering the bottom, which weakens the convective heat transfer intensity and forms a small region of high heat transfer. The normalized average heat transfer coefficient on the squealer floor reduces by 40.26% compared to the cavity depth of 1%H. The position of the maximum value gradually moved to the trailing edge with the cavity depth increasing. Even so, the deepened cavity enlarges the surface of rim, which results in overall heat load increases, and it can be effectively changed by reducing the local region with a high heat transfer coefficient.

(5) Deep-scale cavity is more effective in inhibiting leakage flow at smaller tip clearance. The enlarged gap diminishes the declining quantity of normalized average h, which reduces at most by about 72.6% for the tip clearance of 1%H. In addition, the heat load on the squealer top is not sensitive to the tip clearance height and cavity depth. Although the deep-scale cavity could reduce the heat flux of the cavity floor, it increases the heat flux of the rim wall, so the overall heat flux of the blade tip increases.

(6) In general, the deep-scale cavity is suitable for turbines with low gas-thermal parameters and tight tip clearance. The squealer tip with deep-scale depth is more suitable for small aircraft engines with low power, such as the turboshaft engine.

Acknowledgements

The authors gratefully acknowledge the financial supports for the project from the National Science and Technology Major Project of China (2017-III-0010-0036), China Postdoctoral Science Foundation (NO.2020TQ0147) and Natural Science Foundation of Jiangsu Province (NO. BK20200454).

References

[1] Bunker R.S., Axial turbine blade tips: function, design, and durability. Journal of Propulsion and Power, 2006, 22(2): 271–285.

[2] Bunker R.S., A review of turbine blade tip heat transfer. Annals of the New York Academy of Science, 2001, 934(1): 64–79.

[3] Sun Q., Ji D., Guo H., Research on gas turbine blade material and Fatigue Creep. Turbine Technology, 2017, 59(2): 81–83.

[4] Booth T.C., Dodge P.R., Hepworth H.K., Rotor-tip leakage Part I: basic methodology. ASME, 1981, Paper 81-GT-71.

[5] Yamamoto A., Interaction mechanisms between tip leakage flow and the passage vortex in a linear turbine rotor cascade. Journal of Turbomachinery, 1988, 110(3): 329–338.

[6] Denton J.D., Loss mechanisms in turbomachines. Journal of Turbomachinery, 1993, 115(4): 621–656.

[7] Azad G.S., Han J.C., Teng S., et al., Heat transfer and pressure distributions on a gas turbine blade Tip. Journal of Turbomachinery, 2000, 122(4): 717–724.

[8] Kwak J.S., Han J.C., Heat transfer coefficients of a turbine blade-tip and near-tip regions. Journal of Thermophysics & Heat Transfer, 2003, 17(3): 297–303.

[9] Azad GM.S., Han J.C., Bunker R.S., Lee C.P., Effect of squealer geometry arrangement on a gas turbine blade tip heat transfer. Journal of Heat Transfer, 2002, 124: 452–459.

[10] Zeng F., Du J., Huang L., et al., An experimental method for squealer tip flow field considering relative casing motion. Chinese Journal of Aeronautics, 2020, 33(7): 1942–1952.

[11] Zeng F., Zhang W., Wang Y., et al., Effects of squealer geometry of turbine blade tip on the tip-leakage flow and loss. Journal of Thermal Science, 2021, 30(4): 1376–1387.

[12] Zhou C., Hodson H., Numerical investigation of thermal performance of unshrouded HP turbine blade tips. International Journal of Turbo & Jet Engines, 2009, 26(4): 277–284.

[13] Kavurmacioglu L., Maral H., Senel C.B., et al., Performance of partial and cavity type squealer tip of a HP turbine blade in a linear cascade. International Journal of Aerospace Engineering, 2018, Article: 3262164.

[14] Yang H., Ching H., et al., Turbine rotor with various tip configurations flow and heat transfer prediction. Journal of Thermophysics & Heat Transfer, 2006, 20(1): 80–91.

[15] Liu J.J., Li P., Zhang C., et al., Flow field and heat transfer past an unshrouded gas turbine blade tip with different shapes. Journal of Thermal Science, 2013, 22(2): 128–134.

[16] Zhong J., Wu W., Han S., Research progress of tip winglet technology in compressor. Journal of Thermal Science, 2021, 30(1): 18–31.

[17] Cui W., Wang X., Yao F., Zhao Q., Liu Y., Liu L., Wang C., Yang L., Effects of width variation of pressure-side winglet on tip flow structure in a transonic rotor. Journal of Thermal Science, 2022, 31(1): 141–150.

[18] Zou Z., Shao F., Li Y., et al., Dominant flow structure in the squealer tip gap and its impact on turbine aerodynamic performance. Energy, 2017, 138: 167–184.

[19] Zou Z., Xuan L., Chen Y., et al., Effects of flow structure on heat transfer of squealer tip in a turbine rotor blade. International Communications in Heat and Mass Transfer, 2020, 114: 104588.

[20] Kim J., Seo W., Chung H., et al., Effect of shelf squealer tip configuration on aerothermal performance of gas turbine blade. International Journal of Thermal Sciences, 2021, 168: 107056.

[21] Yan X., Huang Y., He K., et al., Numerical investigations into the effect of squealer-winglet blade tip modifications on aerodynamic and heat transfer performance. International Journal of Heat & Mass Transfer, 2016, 103: 242–253.

[22] Choi S.M., Bang M., Moon H., et al., Wake effects on heat transfer from a turbine blade tip with different configurations and its corresponding shroud. International Communications in Heat and Mass Transfer, 2021, 126: 105333.

[23] Du K., Li Z., Li J., et al., Influences of a multi-cavity tip on the blade tip and the over tip casing aerothermal performance in a high-pressure turbine cascade. Applied Thermal Engineering, 2019, 147: 347–360.

[24] Jiang S., Li Z., Li J., et al., Effects of the novel rib layouts on the tip leakage flow pattern and heat transfer performance of turbine blade. Proceedings of the Institution of Mechanical Engineers Part G: Journal of Aerospace Engineering, 2020, 234(8): 1446–1459.

[25] Lee S.W., Chae B.J., Effects of squealer rim height on aerodynamic losses downstream of a high-turning turbine rotor blade. Experimental Thermal & Fluid Science, 2008, 32(8): 1440–1447.

[26] Zhou C., Effects of endwall motion on thermal performance of cavity tips with different squealer width and height. International Journal of Heat and Mass Transfer, 2015, 91: 1248–1258.

[27] Shi W., Chen P., Li X., et al., Uncertainty quantification of the effects of squealer tip geometry deviation on aerothermal performance. Proceedings of the Institution of Mechanical Engineers Part A Journal of Power and Energy, 2020, 234(7): 1026–1038.

[28] Kwak J., Ahn J., Han J., Effects of rim location, rim height, and tip clearance on the tip and near tip region heat transfer of a gas turbine blade. International Journal of Heat and Mass Transfer, 2004, 47(26): 5651–5663.

[29] Zhou C., Hodson H., Squealer geometry effects on aerothermal performance of tip-leakage flow of cavity tips. Journal of Propulsion and Power, 2012, 28(3): 556–567.

[30] Park J., Lee D., Rhee D., et al., Heat transfer and film cooling effectiveness on the squealer tip of a turbine blade. Energy, 2014, 72: 331–343.

[31] Sakaoglu S., Kahveci H.S., Effect of cavity depth on thermal performance of a cooled blade tip under rotation. International Journal of Heat and Mass Transfer, 2019, 143: 118561.

[32] Bang M., Choi S., Sohn H., et al., Effects of unsteady wakes on heat transfer of blade tip and shroud. International Communications in Heat and Mass Transfer, 2018, 97: 125–135.

[33] Senel C.B., Maral H., Kavurmacioglu L.A., et al., An aerothermal study of the influence of squealer width and height near a HP turbine blade. International Journal of Heat & Mass Transfer, 2018, 120: 18–32.

[34] Kwak, J.S., and Han, J.C., Heat transfer coefficient on a gas turbine blade tip and near tip regions. AIAA-2002-3012, 2002. DOI: 10.2514/6.2002-3012.

[35] Timko L.P., Energy efficient engine high pressure turbine component test performance report, 1984.

[36] Moore J., Moore J.G., Entropy production rates from viscous flow calculations: Part I A turbulent boundary layer flow. Proc. ASME 1983 International Gas Turbine Conference and Exhibit, 1983, V001T001A032. DOI: 10.1115/83-gt-70.

[37] Kwak J., Han J., Heat transfer coefficient on the squealer tip and near squealer tip regions of a gas turbine blade. Journal of Heat Transfer, 2003, 125(4): 669–677.

[38] Ye M., He K., Yan X., Influence of wear damages on aerodynamic and heat transfer performance in squealer tip gap. Applied Thermal Engineering, 2019, 159: 1–19.

[39] Ameri A.A., Steinthorsson E., Rigby D.L., Effect of squealer tip on rotor heat transfer and efficiency. Journal of Turbomachinery, 1998, 120(4): 753–759.

[40] Yang D.L., Feng Z.P., Tip leakage flow and heat transfer predictions for turbine blades. Proceedings of ASME Turbo Expo, 2007, ASME, Paper GT2007-27728.

[41] He K., Investigation of film cooling and heat transfer on a turbine blade squealer tip. Applied Thermal Engineering, 2017, 110: 630–647.

[42] Li F., Wang H., Liu Z., et al., Comparisons of blade tip phantom cooling effectiveness for two tip structures with three tip clearances. Applied Thermal Engineering, 2022, 202: 1–14.